International Journal of Speleology	50 (2)	121-135	Tampa, FL (USA)	May 2021

Available online at scholarcommons.usf.edu/ijs

International Journal of Speleology

Official Journal of Union Internationale de Spéléologie

Bacteria, guano and soot: Source assessment of organic matter preserved in black laminae in stalagmites from caves of the Sierra de Atapuerca (N Spain)

Joeri Kaal [1*], Virginia Martínez-Pillado[2], Antonio Martínez Cortizas [3], Jorge Sanjurjo-Sánchez [4], Arantza Aranburu [5], Juan L. Arsuaga [2,6], and Eneko Iriarte [7]

[1]Pyrolyscience, Calle Vallehermoso 15, 28015 Madrid, Spain
[2]Centro Mixto UCM-ISCIII sobre Evolución y Comportamiento Humanos, Av. Monforte de Lemos, 5, Pabellón 14. 28029, Madrid, Spain
[3]EcoPast (GI-1553), Facultade de Bioloxía, Rua Lope Gómez de Marzoa s/n, 15782 Santiago de Compostela, Spain
[4]Instituto Universitario de Xeoloxía, Universidade da Coruña. ESCI, Campus de Elviña, 15071 A Coruña, Spain
[5]Dpto Geología, Facultad de Ciencia y Tecnología, UPV/EHU. Barrio Sarriena s/n. 48940, Leioa, Bizkaia, Spain
[6]Dpto Paleontología, Facultad de Geología, Universidad Complutense de Madrid. C/José Antonio Novais, 12, 28040 Madrid, Spain
[7]Laboratorio de Evolución Humana, Dpto. Historia, Geografía y Comunicación, Universidad de Burgos, P. Misael Bañuelos, Edificio I+D+i, 09001 Burgos, Spain

Abstract: Speleothems are a recognized source of palaeoclimatic information, but their value as a source of signals from human activities in caves with an archaeological record has rarely been explored. Previous studies of speleothems in the Sierra de Atapuerca karst system (Burgos, northern Spain) revealed an important human fossil record, provided information about human activities in and around these caves, and the impacts on their natural environment. The present study reports the results of molecular characterization of dark-coloured laminae from the stalagmites *Ilargi* (Galería de las Estatuas) and *GS1*, *GS2*, and *GS3* (Galería del Silo), by pyrolysis-GC-MS (Py-GC-MS) and thermally assisted hydrolysis and methylation (THM-GC-MS). The features of the organic matter demonstrate the presence of 1) a dominant aliphatic fraction probably from *in situ* bacterial and *ex situ* plant-derived lipids, 2) black carbon (from soot and/or charcoal), 3) polysaccharides and N-rich moieties (probably from bat guano and microbial sources), and 4) a signal of terpenoid derivatives that may originate from the overlying limestone (kerogen) and extant gymnosperm resin (soils) or cyanobacteria (cave). Some plant-derived lignin may be present as well but was not identified unambiguously. It is concluded that this approach allows identifying multiple general sources of organic matter which can help understand speleothem formation processes, and evidence of soot deposition could be clearly linked to human activities.

Keywords: speleothem, black laminae, organic geochemistry, molecular composition, analytical pyrolysis

Received 19 February 2021; Revised 26 March 2021; Accepted 26 March 2021

Citation: Kaal, J., Martínez-Pillado, V., Martínez Cortizas, A., Sanjurjo-Sánchez, J., Aranburu, A., Arsuaga, J.L., Iriarte, E., 2021. Bacteria, guano and soot: Source assessment of organic matter preserved in black laminae in stalagmites from caves of the Sierra de Atapuerca (N Spain). International Journal of Speleology, 50(2), 121-135.
https://doi.org/10.5038/1827-806X.50.2.2382

INTRODUCTION

The Sierra de Atapuerca karst system in the Iberian Peninsula is a treasure of information on early hominin evolution. Its archaeological and paleontological sites contain some of the most exceptional human fossil accumulations and stone artifacts from the Pleistocene (Carbonell et al., 1995; Arsuaga et al., 1997; Bermúdez de Castro et al., 1997) to the Middle Ages (Falguères et al., 2001; Carbonell et al., 2008; Carretero et al., 2008). The most famous sites correspond to chronologies of the Lower and Middle Pleistocene (e.g., Gran Dolina, Sima del Elefante), containing the oldest hominin remains in Europe (Carbonell et al., 2008). However, research is not limited to Pleistocene events, as some of the galleries of the karst system harbor information on Upper Pleistocene and Holocene paleoenvironments and more recent human activities (Ortega Martínez, 2009; Vergès et al., 2016). The El Portalon de Cueva Mayor archaeological site at the cave entrance, the Galería de las Estatuas and the Galería del Silo are examples of such cavities. In these galleries, detrital deposits as well as stalagmites have been studied (Carretero

*joeri@pyrolyscience.com

et al., 2008; Ortega Martínez, 2009; Aranburu et al., 2012; Martínez-Pillado et al., 2014; Arsuaga et al., 2017).

Speleothems have complex development/erosion histories and the study of the growth dynamics can provide a vast body of information about the environmental conditions during their formation. This is reflected by the stalagmites in the Galería de las Estatuas and the Galería del Silo, showing numerous differences in colour, crystallography and composition (Martínez-Pillado et al., 2014; Fig. 1). The stalagmite *Ilargi* from Galería de las Estatuas has been extensively studied (Martínez-Pillado et al., 2014) and its formation chronology, developed from U-Th series, shows its growth during the last ca. 14,000 yrs, with exception of a hiatus around 12,000–8,000 cal BP. Several techniques, such as the petrographic analysis and scanning electron microscopy equipped with energy dispersive X-ray analysis (SEM-EDS), showed black-colored laminae containing guano remains (hydroxylapatite), others containing soot, and at one level a large charcoal fragment was encountered (^{14}C dated to ca. 7,800 cal BP). The chronology of the *Ilargi* formation was successfully coupled to results from palynological studies from El Portalón archaeological site and a reconstruction of climatic conditions and human activities was based on the comparison of both records: the pollen in detrital sequence and the petrographic analysis of the stalagmite (Martínez-Pillado et al., 2014).

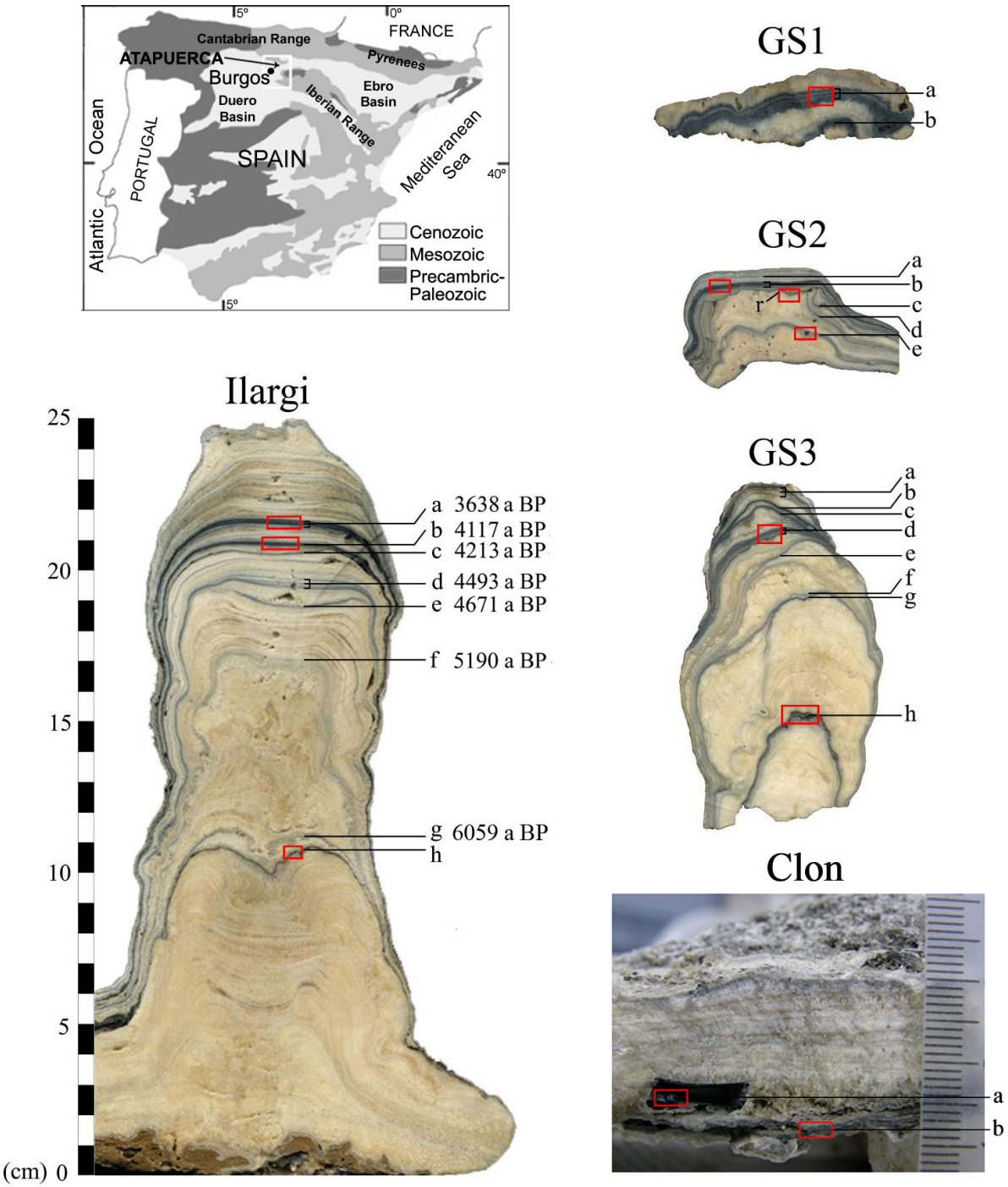

Fig. 1. Cross-sections of the speleothems studied in the present study, from Galería de las Estatuas (*Ilargi* and *Clon*) and Galeria del Silo (*GS1*, *GS2*, *GS3*). Alphabetic denominators correspond to black laminae (Martínez-Pillado et al., 2014). Red squares indicate samples studied here. In *Ilargi*, a chronology for each black laminae (Fig. 1a-g) has been calculated with the StalAge program (Scholz & Hoffmann, 2011) based on the ages published by Martínez-Pillado et al. (2014).

Several methods can be used to obtain paleoenvironmental information from organic matter (OM) in speleothems (review by Blyth et al., 2008). Molecular-scale OM analysis in speleothems has focused on total lipid extracts using gas or liquid chromatography (GC, LC, etc.) in combination with mass spectrometry (MS) (e.g., Rousseau et al., 1995; Blyth & Frisia, 2008; Huang et al., 2008; Rushdie et al., 2011; Yang et al., 2011; Fairchild & Baker, 2012; Blyth & Schouten, 2013). Most studies were concerned with speleothem formation processes and paleoenvironmental reconstructions on the basis of information on markers of vegetation change and temperature records (Blyth et al., 2015). To study macromolecular OM, spectroscopic techniques such as FTIR spectroscopy (Wynn & Brocks, 2014; and references therein) or techniques that involve the chemical and/or thermal degradation of large molecules to GC-amenable building blocks, can be employed. The latter family include conventional analytical pyrolysis (pyrolysis-GC-MS; Py-GC-MS) and thermally assisted hydrolysis and methylation (THM-GC-MS, sometimes referred to as thermochemolysis). Using THM-GC-MS, it was shown that a stalagmite from NW Scotland was prolific of lignin phenols (Blyth & Watson, 2009). A wide range of methoxybenzenes, 1,2-dimethoxybenzenes and 1,2,3-trimethoxybenzenes were detected, indicative of plant-derived lignin in a good preservation state. In such examples, speleothem OM can contain all the macromolecular constituents present in plant tissues and the soil microbial community, such as polysaccharides, lignin, proteins, chitin, or tannin. Abundance of lignin derivatives was also reported for speleothems in several Chinese caves using Py-GC-MS (Hou et al., 2004) and by Heidke et al. (2018) using a microwave-assisted alkaline cupric oxide (CuO) oxidation method applied to a stalagmite and drip water from a cave in Germany. Hou et al. (2004) also distinguished lignin from C3- and C4-plants by means of Py-GC-isotope ratio-MS (Py-GC-IRMS). Blyth et al. (2010) found traces of plant-derived lignin in 3 million yrs old Australian stalagmites using THM-GC-MS, even though these samples did not provide extractable lipid signatures. Using laser-Py-GC-MS, Blyth et al. (2015) studied OM in dissolved OM (DOM) from the calcite crystal matrix, detrital inclusions and lithified guano (from birds and bats), and described the features of their pyrolyzates, including alkane chain length patterns, presence of polysaccharides products (furans) and protein markers such as pyrroles (yet not chitin markers; suggesting that the guano was possibly not from an insectivore). Miller et al. (2016) applied conventional Py-GC-MS, THM-GC-MS and Py-GC-IRMS of coralloid speleothems from Easter Island (Chile). They found alkanes, alkenes, alkylbenzenes, polycyclic aromatic hydrocarbons (PAHs) and N-compounds using Py-GC-MS, and mainly fatty acid methyl esters (FAMEs) using THM-GC-MS. Organic matter sources identified were plant remains and microorganisms. Regarding non-calcitic speleothems, Miller et al. (2020) found evidence of pyrogenic OM in siliceous speleothems from volcanic caves (Hawaii, Azores, Canary Island), and Gonzalez-Pimentel et al. (2018) in yellow colored mats developing on coralloid speleothems in a lava tube from La Palma Island. Sanjurjo-Sánchez et al. (2021) found diverse sources in Al-rich speleothems developed in a granitic rock cave in NW Spain, including microbial chitin and polysaccharides, pyrogenic OM, plant-derived polysaccharides and lignin, and diterpenoids of unidentified source. There is a clear potential for these techniques to identify sources of OM and couple that information to biogeochemical processes within cave systems. This is relevant information, as there is considerable uncertainty on the importance of the major OM sources (air, water, faunal transport, and autochthonous production) in speleothems in different environments (Blyth et al., 2008).

The present study explores the potential of molecular characterization of OM present in various stalagmites from karst sites in the Sierra de Atapuerca. For this purpose, Py-GC-MS and THM-GC-MS were employed on samples from the Galería de las Estatuas and the Galería del Silo, focusing on black-colored laminae.

MATERIALS AND METHODS

Geological setting and speleothem descriptions

The Sierra de Atapuerca is located in the north centre of the Iberian Peninsula, 15 km east of the city of Burgos (see map in Martínez-Pillado et al., 2014). This low-altitude ridge (1,078 m), in the Arlanzón River Valley, contains a large number of karstic cavities formed in Upper Cretaceous limestone that encompasses the multi-level Cueva Mayor-Cueva del Silo karst system comprised by 3,700 m of different-sized galleries and chambers (Ortega Martínez, 2009). These cavities have distinct terrigenous, chemical and anthropic sedimentary infillings covering from the Lower Pleistocene (1.4 Ma) to the Middle Ages (Falguères et al., 2001; Carbonell et al., 2008).

Speleothems from two galleries of the karst system were sampled, i.e., Galería de las Estatuas and Galería del Silo. In both galleries, the presence of abundant storage pits and cave paintings, including numerous Neolithic to Bronze Age archaeological remains (e.g., charcoal, pottery and bone fragments), are evidence of human activity during the recent Prehistory (Ortega Martínez, 2009). Speleothems are widespread in the endokarstic sedimentary sequence that fills these galleries. The most modern and superficial speleothem phase postdates the detrital filling, forming a centimetric flowstone distributed throughout the room, on which abundant stalagmites were formed during the late Pleistocene and Holocene (Martínez-Pillado et al., 2014). Four of these speleothems were selected for the present study (selection of 11 samples): *Ilargi*, *GS1*, *GS2*, and *GS3* (Fig. 1), corresponding to the last speleothem precipitation phase in the Cueva Mayor karst. The *Ilargi* stalagmite was collected from the north end of the Galería de las Estatuas, and its chronology covers from 14 to 3.1 ka BP (Martínez-Pillado et al., 2014). The speleothems *GS1*, *GS2*, and *GS3* were collected from Galería del Silo. Finally, the *Clon* section is actually a lateral cut

of the *Ilargi* stalagmite, taken near a large charcoal fragment dated to 7,800 yr cal BP (Martínez-Pillado et al., 2014).

Light-cream colors predominate in the studied speleothems, with dark bands formed by alternating black laminae (Fig. 1) that are more abundant and thicker in the upper half of all the stalagmites. Based on the different petrological and compositional features, two types of black layers have been identified; those with erosive surfaces that show the presence of hydroxylapatite precipitate, and those characterized by the absence of erosional features and formed by the accumulation of soot particles that cover the calcite crystals (photographs in Martínez-Pillado et al., 2014). Erosive black layers correspond to levels *Ilargi-h* and *GS3-h* stalagmites, and *GS1-b* (Fig. 1). Non-erosive black layers correspond to all the other samples except *GS2-r*, which belongs to a clear mechanical fracture of anthropic origin with soot evidence (Fig. 1).

Sample preparation

After cutting the speleothems longitudinally, their surfaces were polished and at the selected sampling points, an abrasion was performed with a tungsten carbide dentist's drill to remove the first millimeters and avoid possible contamination.

Carbonates were eliminated by addition of aliquots of 5% HCl (aq) until the reaction was complete. Next, 40 ml of 1 M HF/HCl solution, equilibrated for 3 hr in an orbital shaker, were used to eliminate reactive minerals that may interfere during pyrolysis (Miltner & Zech, 1997). The supernatant was discarded and the residue washed by repeated (four times) additions of 40 ml of distilled water followed by centrifugation and decantation. Finally, the residue was dried for 24 h at 50°C.

Analytical pyrolysis

For conventional pyrolysis (Py-GC-MS), the dried residues were inserted into quartz tubes with quartz wool at both ends and pyrolyzed using a CDS Pyroprobe 5250 for 10 s at 750°C (10°C ms^{-1} heating rate) with both the valve oven and the transfer line held isothermal at 325°C. This high pyrolysis temperature was used to promote the release of products from thermally relatively stable OM such as soot and charcoal (Kaal et al., 2009). Pyrolysis products were separated on a 6890N gas chromatograph (Agilent Technologies) operating in splitless mode to maximize signal intensity, using helium carrier gas (1 ml min^{-1}) and a HP-5MS polysiloxane-based (phenyl, 95% dimethylpolysiloxane column) column (30 m length, 0.25 mm i.d., film thickness 0.25 µm). The oven program started at 50°C (1 minute) and finished, after heating 20°C min^{-1}, at 325°C (4 min). The detector (Agilent 5975) operated at 70 eV electron impact (m/z 50–500). Quantification of pyrolysis products was based on the peak area of dominant fragment ions. The relative proportions of each pyrolysis product were calculated as the percentage of the sum of all peak areas (total quantified peak area, TQPA). Several samples produced chromatograms of which the signal-to-noise ratio was too low for a reliable assessment of the pyrolysis fingerprint (*Ilargi-a*, *Clon-a*), mainly because of the virtually complete digestion during the HF/HCl treatment (indicating scarce and/or labile organic constituents).

Two samples with relatively high yield of residue after the HCl/HF treatment (*Ilargi-h* and *GS3-h*), and sample *GS2-b*, were analysed with THM-GC-MS by addition of droplets of 25% aqueous tetramethylammonium hydroxide (TMAH, 25%), followed by analysis under the same conditions as for Py-GC-MS. The TMAH was added twice, with an evaporation step at 35°C in between. The THM-GC-MS data was evaluated qualitatively (no quantification based on peak areas).

RESULTS AND DISCUSSION

Pyrolysis-GC-MS

Products based on a polymethylene chain (methylene chain compounds; MCC) are the most abundant in all samples (54 ± 11%; Fig. 2). Within this group, homologous series of *n*-alkane/*n*-alkene pairs (Table 1) prevail (53 ± 11% of TQPA). Among the *n*-alkenes, there is a gradual decrease in the relative proportion with chain length, with a minor maximum at C_{14} and C_{16} alkene, with the exception of the *Clon-b* sample, which has another maximum in the C_{25}-C_{27} range. The average chain length of the *n*-alkanes is 18 ± 2, and that of the *n*-alkenes is 14 ± 2 (Fig. 3). *n*-alkenes are unusually dominant over *n*-alkanes (alkane/alkene ratio of 0.3 to 0.7), except for *Clon-b* (ratio of 1.8; Fig. 3). Minor proportions of branched alkanes, alkadienes and C_{16} and C_{18} alkylnitriles were detected as well – the latter of which only in samples *Ilargi-b* and *Ilargi-h* (Fig. 3). The MCC are least abundant in the sample *Ilargi-h*. The potential sources of these products are diverse, such as insect cuticles, plant leaf epicuticular waxes (especially long-chain alkanes), and all sorts of arrangements of free/esterified and macromolecular fatty acids (pyrolytically decarboxylated) in for instance algaenan, cutin, suberin, cutan, and suberan (e.g., Nip et al., 1986; Tegelaar et al., 1989; Quénéa et al., 2006). Some information on the sources of the MCC was obtained by THM-GC-MS (see below), which preserves carboxylic functionalities (Challinor, 1991).

The second most abundant class are the monocyclic aromatic hydrocarbons (MAHs; 21 ± 5.4%; Fig. 2), composed of alkylbenzenes with one (toluene) to seven C atoms in side-chain(s). Identifying the origin of the MAHs is difficult as they are potential products of many sources. Considering the abundance of MCC, for the MAHs with ≥4 C atoms in alkyl side-chains, the most likely source is cyclization of MCC structures during analytical pyrolysis (Sáiz-Jiménez, 1994). The MAHs with 1-3 C atoms in side chains can be products of degraded lignin, but a mixed source of microbial OM (especially in case of toluene) and cyclization products is more likely in this case as lignin is scarce (see below). For toluene, another potential source is pyrogenic OM (Kaal et al., 2009). Benzene, another major MAH product of pyrogenic OM, was not quantified due to poor peak resolution in the earliest section of the chromatograms.

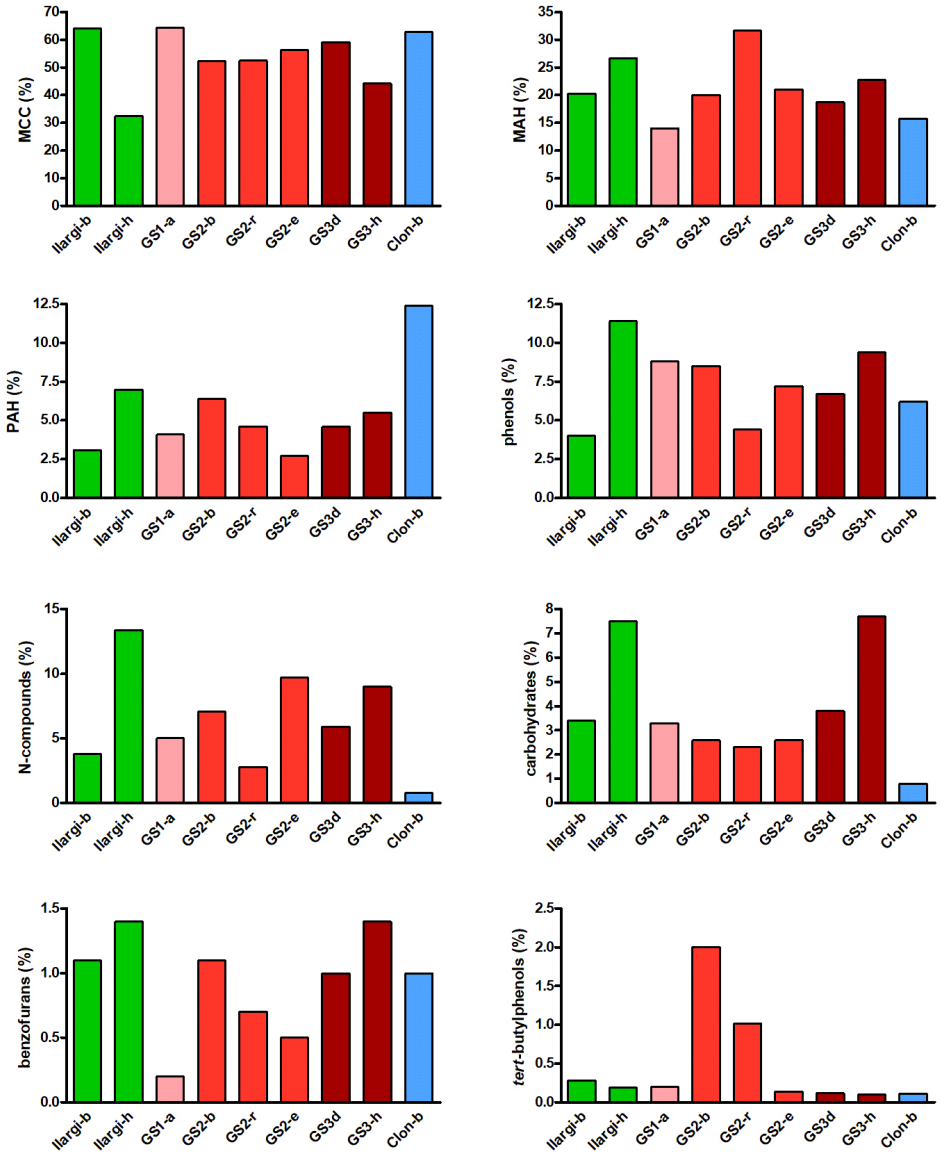

Fig. 2. Relative proportions of the main Py-GC-MS compound groups, in percentage of total quantified peak area (% TQPA). MCC=methylene chain compounds, N-compounds = nitrogen-containing compounds, MAH/PAH= monocyclic/polycyclic aromatic hydrocarbons. Colors represent stalagmites (*Ilargi* in green, *GS1* in pink, *GS2* in red, *GS3* in garnet and *Clon* in blue).

Table 1. List of pyrolysis-GC-MS products and relative abundance (as percentage of total quantified peak area; % TQPA), identified in the black laminae of the speleothems from the Sierra de Atapuerca (RT: retention time; *m/z*: mass-charge of ions used for semi-quantitation; BF: benzofurans; CARB: carbohydrate products; CONT: contamination; MAH: monocyclic aromatic hydrocarbon; MCC: methylene chain compounds; NCOMP: nitrogen-containing compounds; PAH: polycyclic aromatic hydrocarbons; PHEN: phenols).

RT (min)	Pyrolysis product	*m/z*	Group	Ilargi-b	Ilargi-h	GS1-a	GS2-b	GS2-r	GS2-e	GS3d	GS3-h	Clon-b
4.561	benzofuran	118+89	BF	0.83	0.92	0.14	0.92	0.73	0.53	0.67	1.00	0.41
6.243	C_2-benzofuran	145+146	BF	0.10	0.15	0.01	0.09	0.00	0.00	0.12	0.14	0.24
6.306	C_2-benzofuran	145+146	BF	0.16	0.36	0.03	0.08	0.00	0.00	0.20	0.29	0.36
3.308	2-cyclopenten-1-one	82+53	CARB	1.15	2.95	0.00	0.00	0.00	0.36	1.13	2.76	0.49
3.331	3/2-furaldehyde	95+96	CARB	1.46	2.88	0.77	0.90	0.00	0.65	1.03	2.51	0.00
3.869	C_1-cyclopentenone	67+96	CARB	0.80	1.71	2.55	1.72	2.33	1.54	1.66	2.43	0.27
8.268	di-*tert*-butylphenol	191+206	CONT	0.28	0.19	0.20	2.01	1.02	0.14	0.12	0.10	0.11
2.839	toluene	91+92	MAH	13.16	17.73	8.19	10.13	20.19	12.08	10.96	14.24	6.60
3.536	C_2-benzene	91+106	MAH	3.01	4.46	2.43	4.10	6.00	3.71	3.04	3.85	3.95
3.593	C_2-benzene	91+106	MAH	1.29	1.76	0.85	1.59	2.64	1.28	1.46	1.51	1.18
4.245	C_3-benzene	91+120	MAH	0.49	0.37	0.26	0.76	0.14	0.60	0.34	0.32	0.31
4.429	C_3-benzene	105+120	MAH	0.57	0.04	0.29	0.47	0.28	0.55	0.56	0.48	0.41
4.550	C_3-benzene	105+120	MAH	0.51	0.96	0.96	1.19	0.89	1.09	1.07	0.81	1.51

4.801	C_3-benzene	105+120	MAH	0.24	0.42	0.61	0.74	0.99	0.53	0.47	0.52	0.93
5.069	alkylbenzene C_4	91	MAH	0.38	0.26	0.29	0.36	0.21	0.38	0.24	0.34	0.18
5.842	alkylbenzene C_5	91	MAH	0.21	0.27	0.15	0.26	0.31	0.31	0.20	0.23	0.48
6.603	alkylbenzene C_6	91	MAH	0.24	0.32	0.00	0.24	0.00	0.21	0.18	0.18	0.10
7.324	alkylbenzene C_7	91	MAH	0.15	0.14	0.00	0.16	0.00	0.25	0.14	0.24	0.14
3.663	alkene C_9	55+56	MCC	5.37	2.56	6.27	2.74	4.74	5.61	5.76	4.27	1.58
4.464	alkene C_{10}	55+56	MCC	4.07	2.57	6.19	3.20	5.18	5.30	6.05	4.41	1.82
5.259	alkene C_{11}	55+69	MCC	3.35	1.59	3.35	2.03	2.39	4.06	3.82	2.51	0.85
6.026	alkene C_{12}	55+69	MCC	3.31	1.54	3.28	1.74	2.40	3.66	3.58	2.36	0.93
6.747	alkene C_{13}	55+69	MCC	3.61	1.46	2.89	2.83	4.48	4.09	3.97	2.96	0.94
7.433	alkene C_{14}	55+69	MCC	5.61	2.47	6.47	3.00	3.75	6.77	7.04	4.33	1.04
8.074	alkene C_{15}	55+69	MCC	2.59	1.38	3.25	3.09	3.99	3.66	3.40	2.25	0.95
8.681	alkene C_{16}	55+69	MCC	4.44	1.55	5.46	1.85	2.59	4.80	4.60	3.11	0.88
9.253	alkene C_{17}	55+69	MCC	1.57	0.63	1.89	0.74	0.99	1.06	2.10	1.21	0.79
9.802	alkene C_{18}	55+69	MCC	0.88	0.78	1.68	0.80	0.67	0.72	0.88	1.24	0.85
10.323	alkene C_{19}	55+69	MCC	0.44	0.39	0.65	0.80	0.66	0.19	0.28	0.54	1.00
10.821	alkene C_{20}	55+69	MCC	0.55	0.40	0.61	0.38	0.53	0.16	0.43	0.53	1.03
11.296	alkene C_{21}	55+69	MCC	0.35	0.23	0.29	0.22	0.38	0.41	0.14	0.24	1.04
11.753	alkene C_{22}	55+69	MCC	0.68	0.35	0.72	1.20	0.28	0.34	0.39	0.16	0.84
12.188	alkene C_{23}	55+69	MCC	0.49	0.20	0.38	0.50	0.37	0.31	0.29	0.32	0.92
12.600	alkene C_{24}	55+69	MCC	0.57	0.21	0.67	0.79	0.62	0.00	0.26	0.08	1.04
13.007	alkene C_{25}	55+69	MCC	0.45	0.33	0.58	0.47	0.36	0.00	0.26	0.33	1.75
13.396	alkene C_{26}	55+69	MCC	0.38	0.36	0.18	0.61	0.28	0.00	0.22	0.21	1.46
13.779	alkene C_{27}	55+69	MCC	0.36	0.23	0.68	0.40	0.14	0.00	0.23	0.26	1.30
14.122	alkene C_{28}	55+69	MCC	0.33	0.27	0.39	0.29	0.28	0.00	0.26	0.20	0.67
14.477	alkene C_{29}	55+69	MCC	0.24	0.17	0.22	0.32	0.14	0.00	0.00	0.17	0.47
14.820	alkene C_{30}	55+69	MCC	0.09	0.00	0.00	0.00	0.00	0.00	0.00	0.00	0.34
15.169	alkene C_{31}	55+69	MCC	0.03	0.09	0.00	0.27	0.00	0.00	0.07	0.00	0.12
7.513	alkadiene (tentative)	55+69	MCC	0.47	0.47	1.39	0.53	0.21	0.33	0.58	0.44	0.09
7.588	alkadiene (tentative)	55+69	MCC	0.34	0.42	1.23	0.42	0.31	0.74	0.14	0.23	0.32
3.726	alkane C_9	57+71	MCC	1.71	0.41	0.43	0.39	0.36	1.02	2.07	0.95	1.31
4.521	alkane C_{10}	57+71	MCC	1.31	0.26	0.78	0.74	0.89	0.69	1.15	0.91	1.11
5.322	alkane C_{11}	57+71	MCC	1.63	0.51	0.57	0.51	0.56	1.02	0.93	0.59	1.26
6.083	alkane C_{12}	57+71	MCC	1.64	0.51	0.60	0.51	0.79	0.79	0.93	0.51	1.42
6.798	alkane C_{13}	57+71	MCC	2.23	0.67	0.98	0.90	1.24	1.39	1.46	0.79	1.32
7.473	alkane C_{14}	57+71	MCC	1.28	0.40	0.48	0.47	0.52	0.58	0.63	0.36	1.45
8.114	alkane C_{15}	57+71	MCC	2.66	0.77	1.63	2.58	2.31	1.93	1.91	0.93	1.49
8.721	alkane C_{16}	57+71	MCC	0.70	0.35	0.57	0.65	0.74	0.59	0.32	0.39	1.43
9.293	alkane C_{17}	57+71	MCC	1.00	0.50	0.59	1.36	1.83	0.75	0.54	0.43	1.35
9.831	alkane C_{18}	57+71	MCC	0.48	0.47	0.43	0.59	0.61	0.41	0.22	0.32	1.71
10.352	alkane C_{19}	57+71	MCC	0.50	0.40	0.47	1.20	0.92	0.69	0.34	0.26	1.72
10.844	alkane C_{20}	57+71	MCC	0.57	0.42	0.87	0.88	0.57	0.86	0.31	0.18	2.20
11.319	alkane C_{21}	57+71	MCC	0.45	0.42	0.65	0.95	0.40	0.24	0.45	0.21	2.25
11.771	alkane C_{22}	57+71	MCC	0.45	0.45	1.05	1.08	0.31	0.22	0.37	0.00	2.32
12.205	alkane C_{23}	57+71	MCC	0.64	0.56	0.79	0.65	0.32	0.46	0.36	0.48	3.01
12.617	alkane C_{24}	57+71	MCC	0.86	0.68	0.82	1.62	0.39	0.32	0.54	0.76	3.14
13.018	alkane C_{25}	57+71	MCC	0.60	0.46	0.79	0.78	0.17	0.11	0.26	0.64	3.12
13.401	alkane C_{26}	57+71	MCC	0.56	0.45	0.93	1.05	0.42	0.36	0.26	0.74	2.63
13.779	alkane C_{27}	57+71	MCC	0.49	0.37	0.39	0.63	0.21	0.22	0.25	0.45	2.24
14.134	alkane C_{28}	57+71	MCC	0.40	0.26	0.53	0.67	0.28	0.00	0.20	0.47	1.37
14.483	alkane C_{29}	57+71	MCC	0.54	0.35	0.41	0.77	0.52	0.00	0.23	0.50	0.98
14.820	alkane C_{30}	57+71	MCC	0.23	0.16	0.31	0.55	0.00	0.00	0.00	0.15	0.46
15.169	alkane C_{31}	57+71	MCC	0.16	0.16	0.00	0.74	0.00	0.00	0.00	0.15	0.31
8.377	branched alkane	57+71	MCC	0.27	0.10	0.27	1.47	1.02	0.65	0.39	0.25	0.15
9.608	branched alkane	57+71	MCC	0.22	0.17	0.24	1.32	1.27	0.76	0.26	0.37	0.07
10.416	alkylnitrile C_{16}	55+57	MCC	0.87	0.75	0.00	0.00	0.00	0.00	0.00	0.00	0.00

11.404	alkylnitrile C_{18}	55+57	MCC	0.99	0.73	0.00	0.00	0.00	0.00	0.00	0.00	0.00
2.727	pyrrole	67	NCOMP	2.02	4.89	2.98	4.71	2.82	6.41	2.92	4.92	0.00
3.370	C_1-pyrrole	80+81	NCOMP	1.19	4.75	2.05	1.63	0.00	3.29	2.87	3.52	0.67
3.551	acetamide	59	NCOMP	0.00	2.67	0.00	0.00	0.00	0.00	0.00	0.00	0.00
4.544	benzonitrile	103+76	NCOMP	0.56	1.06	0.00	0.76	0.00	0.00	0.14	0.54	0.17
4.990	indene	115+116	PAH	0.61	1.42	0.63	0.90	0.81	0.71	1.11	1.14	0.52
5.820	C_1-indene	115+130	PAH	0.29	0.87	0.80	0.63	0.21	0.38	0.65	0.62	0.53
5.877	C_1-indene	115+130	PAH	0.23	0.69	0.65	0.45	0.24	0.53	0.52	0.59	0.39
6.123	naphthalene	128	PAH	0.30	0.37	0.16	0.55	0.60	0.21	0.22	0.46	0.22
6.907	C_1-naphthalene	142+115	PAH	0.24	0.40	0.07	0.52	0.28	0.25	0.29	0.32	0.44
7.033	C_1-naphthalene	142+115	PAH	0.22	0.41	0.31	0.39	0.42	0.38	0.34	0.32	0.57
7.485	biphenyl	154	PAH	0.07	0.19	0.00	0.03	0.28	0.00	0.01	0.04	0.18
7.662	C_2-naphthalene	156+141	PAH	0.15	0.16	0.26	0.21	0.10	0.09	0.16	0.26	0.54
7.752	C_2-naphthalene	156+141	PAH	0.28	0.54	0.44	0.59	0.81	0.08	0.25	0.52	1.80
8.463	C_3-naphthalene	155+170	PAH	0.08	0.16	0.20	0.16	0.07	0.00	0.15	0.14	0.44
8.658	C_3-naphthalene	155+170	PAH	0.13	0.23	0.20	0.30	0.14	0.00	0.29	0.22	1.61
8.824	C_3-naphthalene	155+170	PAH	0.07	0.14	0.18	0.24	0.07	0.00	0.03	0.10	0.83
8.784	C_4-naphthalene	169+184	PAH	0.00	0.12	0.00	0.00	0.00	0.00	0.00	0.00	0.34
8.915	C_4-naphthalene	169+184	PAH	0.00	0.12	0.00	0.00	0.00	0.00	0.00	0.00	0.18
8.996	C_4-naphthalene	169+184	PAH	0.00	0.13	0.00	0.00	0.00	0.00	0.00	0.00	0.17
9.360	C_4-naphthalene	169+184	PAH	0.03	0.20	0.03	0.16	0.00	0.03	0.01	0.03	0.31
9.413	C_4-naphthalene	169+184	PAH	0.03	0.08	0.01	0.14	0.00	0.00	0.09	0.06	0.43
9.516	C_4-naphthalene	169+184	PAH	0.02	0.04	0.00	0.11	0.00	0.00	0.04	0.08	0.19
9.671	C_4-naphthalene	169+184	PAH	0.05	0.22	0.00	0.15	0.00	0.00	0.04	0.12	0.65
8.818	fluorene	166+165	PAH	0.18	0.41	0.06	0.31	0.10	0.00	0.25	0.35	0.13
9.337	cadalene	183+198	PAH	0.10	0.04	0.11	0.39	0.28	0.00	0.13	0.15	1.90
9.997	phenanthrene	178	PAH	0.06	0.11	0.00	0.15	0.21	0.00	0.00	0.00	0.06
4.521	phenol	94+66	PHEN	2.30	6.21	5.49	5.86	4.38	5.19	4.03	6.76	2.79
5.082	C_1-phenol	107+108	PHEN	0.54	1.33	0.88	0.80	0.00	0.75	1.08	1.05	1.49
5.271	C_1-phenol	107+108	PHEN	1.19	3.82	2.43	1.83	0.00	1.22	1.63	1.56	1.94

Polycyclic aromatic hydrocarbons (PAHs; 5.6 ± 2.9%; Fig. 2) include series of indenes (C_0-C_3) and naphthalenes (C_0-C_5), in addition to fluorene, biphenyl and phenanthrene/anthracene (co-eluted isomers). Again, several sources can be highlighted, depending on the substitution (alkylation) patterns. Firstly, the (poly)alkyl-PAHs originate primarily from a terpenoid-like material (e.g., resins and essential oils), while the unsubstituted PAHs originate mainly, but not exclusively, from pyrogenic OM (Hatcher & Clifford, 1997; González-Vila et al., 2001; Kaal et al., 2016). For the C_5-alkylnapthalene with *iso*-C_3-configuration (probably 1,6-dimethyl-4-isopropylnaphthalene, i.e., cadalene), a non-terpenoid source of pyrogenic OM is impossible as charring does not create isopropyl groups. This compound is most abundant in the sample *Clon-b* (Fig. 3). It is a pyrolysis dehydration product of cadinenes (Van Aarssen et al., 1994; Hatcher & Clifford, 1997) in higher plants, i.e., from resins from local vegetation, or a leaking component of the dolomite rock (kerogen), either way entering the cave through dripping water. However, a bacterial source cannot be discarded (Romero-Sarmiento et al., 2010). The residues of incomplete combustion (charcoal and soot) are known to produce C_1-alkyl-PAHs (methylnaphthalenes), minor proportions of C_2- and sometimes C_3-C_4-alkyl-PAHs, usually in decreasing proportions as the number of alkyl C atoms increases (opposite trend for terpenoid products). Following this rationale, pyrogenic OM (charcoal/soot) would account for the majority of the naphthalene, fluorene, biphenyl and phenanthrene/anthracene, a smaller proportion of the methylnaphthalenes and negligible amount of higher substitution levels, and *vice versa* for the terpenoid-like precursors. Figure 3 shows the sum of unsubstituted PAHs (excluding indene) and the ratio of unsubstituted PAHs to alkyl-PAHs, which provide an indication of the abundance of pyrogenic OM and the balance between pyrogenic and terpenoid-derived OM, respectively.

Other classes of compounds are carbohydrate products (3.8 ± 2.3%; Fig. 2), consisting of cyclopentenones and 3/2-furaldehyde; N-containing compounds (6.4 ± 3.9%) such as pyrrole, C_1-pyrrole, acetamide and benzonitrile; phenols (7.4 ± 2.4%); benzofurans (0.9 ± 0.4%) and a di-*tert*-butylphenol contamination (0.5 ± 0.6%). The carbohydrates probably originate from a combination of plant-derived and microbial polysaccharides. The N-compound acetamide is a product of chitin and/or peptidoglycan in cell wall materials in fungi and bacteria, or exoskeleta of arthropods (Stankiewicz et al., 1996; Gupta & Cody, 2011). It was only detected in sample *Ilargi-h* (Fig. 3), but this may reflect that the chitin/peptidoglycan in that sample is relatively well-preserved rather than absent in the other samples. This compound can be related to disintegration of guano from insectivorous animals (Stankiewicz et al.,

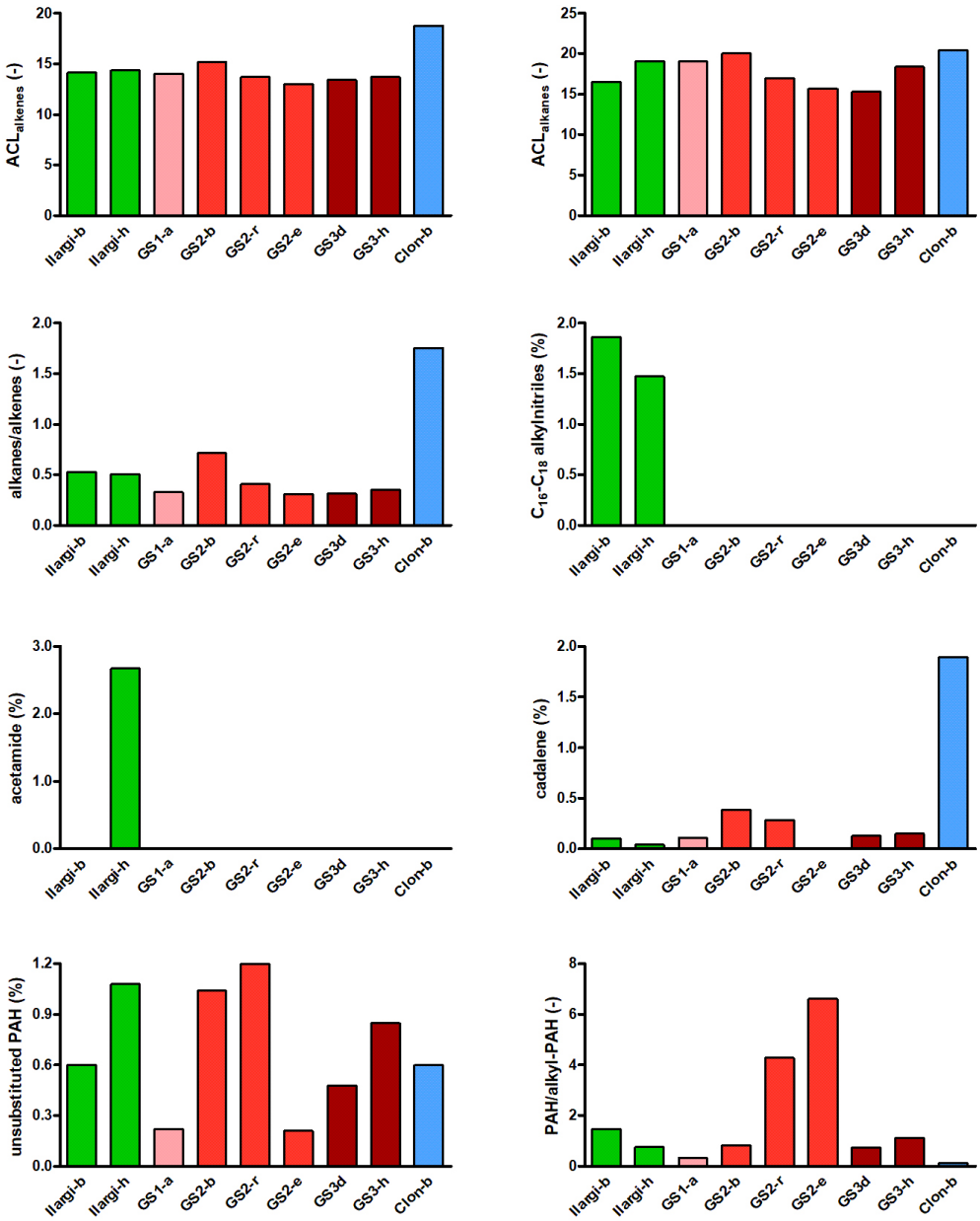

Fig. 3. Parameters from Py-GC-MS used to describe pyrolyzate compositions. ACL= average chain length (of *n*-alkanes and *n*-alkenes), PAH= polycyclic aromatic hydrocarbons. Colors represent stalagmites (*Ilargi* in green, *GS1* in pink, *GS2* in red, *GS3* in garnet and *Clon* in blue).

1996) and their presence in this layer is compatible with the phosphatic minerals detected under SEM-EDS (Martínez-Pillado et al., 2014). The benzofurans are not specific of any source, but in the light of the pyrolyzate composition, a source in carbohydrates and pyrogenic OM (including charred carbohydrates) seems likely (Boon et al., 1994; Pastorova et al., 1994). The absence of significant peaks of lignin products (e.g., methoxyphenols) in pyrolyzates (Sáiz-Jiménez & de Leeuw, 1986), suggests that the phenols should be ascribed to microbial OM (e.g., proteins), but THM-GC-MS showed several peaks of possible lignin products, and it is known that Py-GC-MS fingerprints of lignin-derived DOM are less easily recognized by Py-GC-MS than lignin from particulate OM (Kaal et al., 2020), which implies that the phenols may also originate from dissolved lignin-derived moieties.

THM-GC-MS

Of the three samples analysed by THM-GC-MS, the chromatogram with the highest signal intensity was sample *Ilargi-h* (Fig. 4). Most of the peaks can be ascribed to compounds with a fatty acid structure, detected as fatty acid methyl esters (FAMEs). The C_{16} and C_{18} FAMEs have the highest peak intensity. Their source, i.e., free or esterified C_{16} and C_{18} fatty acids, are omnipresent in nature and a specific origin cannot be determined, but some minor FAME products provide clues on the composition and source of the dominant polymethylene aliphatic OM. For instance, C_{15} FAMEs included not only *n*-C_{15} FAME but also branched-chain (*iso*/*anteiso*) C_{15} FAMEs, which is indicative of (bacterial) membrane lipids (Ratledge & Wilkinson, 1988; Kaneda, 1991; Spaccini et al., 2013), for instance in cave bacterial communities (Blyth & Frisia, 2008), among which cyanobacteria (Cox et al., 1989a) and lipids in bat guano (Queffelec et al., 2018).

Furthermore, a series of even-numbered long-chain FAMEs (C_{20}-C_{28}) probably indicate fungal or bacterial wax esters, or (geopolymerized) epicuticular plant waxes (Ratledge, 1997; De Leeuw et al., 2006). Absence of unequivocal lignin products, as is the

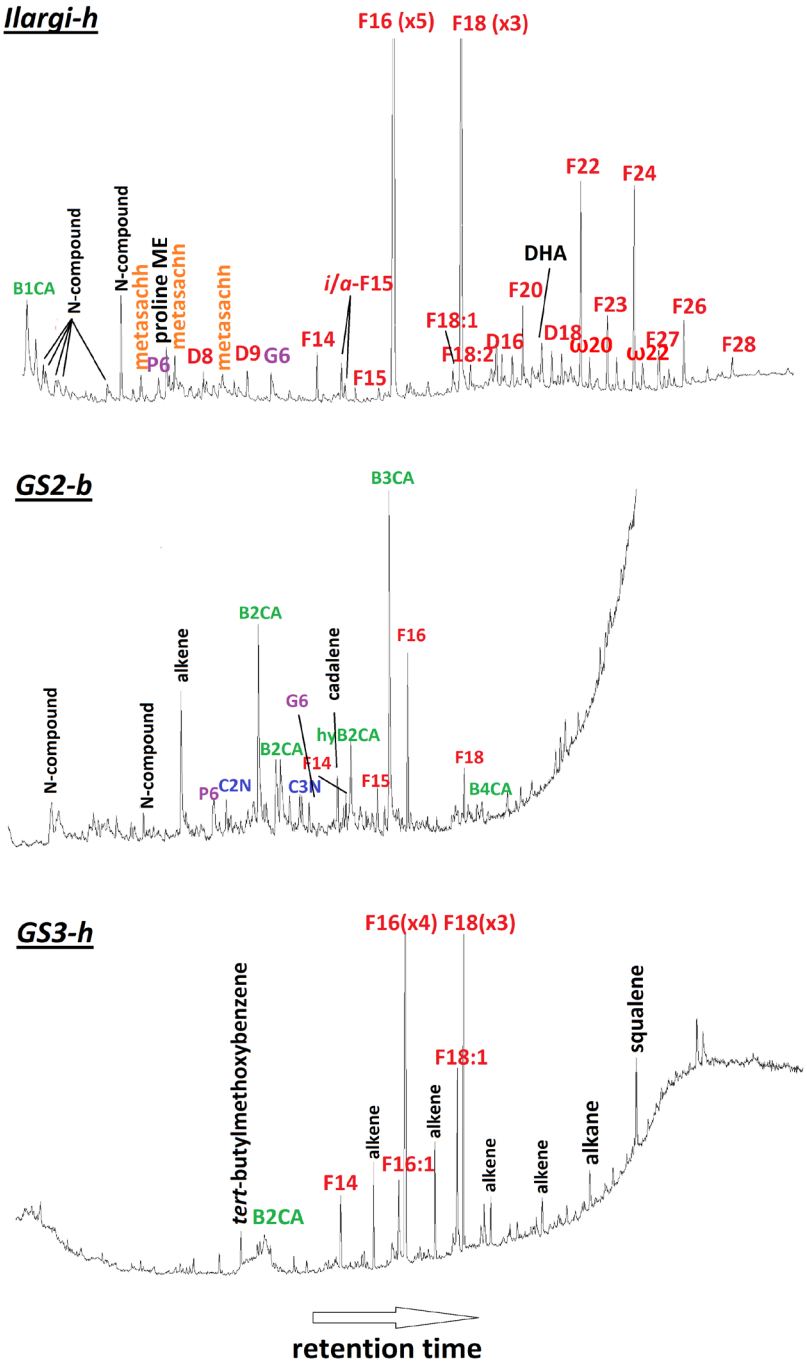

Fig. 4. THM-GC-MS total ion current chromatograms of the three samples analyzed by this method. Chain length number of polymethylene compounds indicated with *n*: F*n* = fatty acid methyl ester (FAME), D*n* = diacid dimethyl ester, ω*n* = ω-methoxy-FAME, *i*/*a* = *iso*/*anteiso* (C_{15} FAME), B*n*CA = benzenecarboxylic acid methyl ester with *n* carboxylic acid methyl ester groups, N-compound = nitrogen-containing compound, P6 = 4-methoxybenzoic acid methyl ester, G6 = 3,4-dimethoxybenzoic acid methyl ester, C_2N/C_3N = dimethyl- and trimethylnaphthalenes.

case for this sample, was interpreted by Queffelec et al. (2018) as a prevailing source of microbial OM to the long-chain even-numbered FAME in bat guano. Some diacids (DAMEs) were detected, but mainly C_{16} and C_{18}, suggesting that suberin (which would reflect root/bark sources) is not a major source of the FAMEs (Kolattukudy, 2001; Nierop & Verstraten, 2004). This is also the main reason why the long-chain FAMEs were not ascribed to suberin, in addition to the lack of evidence of particulate plant-derived OM. Other detected FAMEs were unsaturated ($C_{18:1}$) FAME and short-chain DAMEs (≤C_9), the latter of which probably result from degradation of the former. It is concluded that the polymethylene OM originates at least in part from bacterial lipids, whereas the contribution of plant-derived OM remains unknown.

Multiple N-containing products were identified in the chromatogram of *Ilargi-h*, including tentatively identified *N*,*N*-dimethylalanine methyl ester (ME; *m*/*z* 72 and 131), *N*-methyl-2,5-pyrrolidinedione (*m*/*z* 56 and 113), 3-phenylpropenoic acid ME (*m*/*z* 131 and 162), several proline and hydroxyproline products including 2-methyl-5-oxo-proline ME, and several other unidentified N-heteroaromatic products (*m*/*z* 108 and 139; *m*/*z* 108 and 138) (Knicker et al., 2001; Lejay et al., 2019). The N-compounds detected are not the typical products of aged microbial OM in soils, which is prolific of alkylindoles and alkylpyrroles after THM. Instead, they originate from a well-preserved N-rich source of local production, such as bat guano proteins (insectivorous, i.e., chitin-containing) and bacteria (peptidoglycan). Note that bats have abundant connective tissues in their wings and tail membranes (Wimsatt, 1970), consisting of the proline rich polymer collagen, so that other remains of bats also form a potential source of the N-products. This might seem far-fetched, but the aforementioned N-heteroaromatic products (*m*/*z* 108 and 139; *m*/*z* 108 and 138) are abundant in the THM-GC-MS chromatograms of collagen (Lejay et al., 2019). Regarding the bacterial source, Actinobacteria, Proteobacteria, and other Gram-negative phylae such as Nitrospirae include genera that are N-fixing chemolithotrophs (Willey, 2008) and are frequently found in cave speleothems (Riquelme et al., 2015; Lavoie et al., 2017; González-Pimentel et al., 2018). Further research would be needed to characterize the relative contributions of these sources of N.

Many carbohydrate products such as methylated C_5- and C_6-metasaccharinic acids were detected (Fabbri & Helleur, 1999). These compounds formed from polysaccharides in plant-, microbial-, or guano-derived OM.

The compounds 4-methoxybenzoic acid ME (P6) and 3,4-dimethoxybenzoic acid ME (G6) may reflect lignin, tannin or another source of phenolic OM (e.g., Nierop & Filley, 2007). Dominance of these acid moieties has been reported for THM-GC-MS chromatograms of DOM (Kaal et al., 2017), so that the absence of more specific markers of lignin does not imply that DOM in soil leachates is not a significant source of these compounds. Some benzoic acid methyl ester (ME) and benzenedicarboxylic acid dimethyl esters (B2CA) were detected, possibly from lignin (Hatcher & Minard, 1995).

Dehydroabietic acid ME (DHA) and other abietic acid derivatives are well-known constituents of conifer resins (Keeling & Bohlmann, 2006). However, the presence of abietane derivatives in samples from the Devonian suggested that abietic acid synthesis

might not be restricted to terrestrial conifers (Romero-Sarmiento et al., 2010) and, more recently, Costa et al. (2016) demonstrated that several genera of cyanobacteria metabolise dehydroabietic and abietic acid as well. This implies that the DHA in this sample may reflect diterpenoids from gymnosperms (soil leachate) or bacterial sources (produced *in situ*). It is important to note that Romero-Sarmiento et al. (2010) also found cadalenes in the same samples, suggesting that perhaps the detected cadalene (THM-GC-MS and Py-GC-MS) may be a product of bacterial biomass as well (see above). The *Ilargi-h* sample corresponds to an accumulation of guano (forming hydroxylapatite; Audra et al., 2019) after an erosion event. Note that this event could be due to biogenic corrosion caused by the guano itself (Audra et al., 2019; Dandurand et al., 2019). Cyanobacterial activity in the guano and rapid movement of water from the soil environment (known to support conifer vegetation around that time; Martínez-Pillado et al., 2014) are both plausible hypotheses.

Sample *GS2-b* gave benzenetricarboxylic acid trimethyl ester (B3CA) as the largest peak, followed by C_{16} FAME, isomers of B3CA and B2CA and some minor peaks of other FAMEs and unidentified N-compounds (Fig. 4). The partial ion chromatogram of *m/z* 279 also shows three isomers of B4CA. These benzene polycarboxylic acid (BPCA) patterns, and in particular the presence of B4CA and the dominance of B3CA over B2CA and B1CA, are indications of oxidized pyrogenic OM in this sample (Kaal et al., 2008). In this case, the three isomers of methoxy-B2CA can probably be ascribed to the same source of pyrogenic OM (Kaal & Filley, 2016). This is in agreement with the abundance of unsubstituted PAHs and the high ratio of unsubstituted PAHs-to-alkyl-PAHs observed with Py-GC-MS (Fig. 3). Hence, whereas the benzenecarboxylic acid patterns of sample *Ilargi-h* did not indicate pyrogenic OM, it seems very likely that charred OM is the main type of OM in *GS2-b*. The presence of N-containing products and C_{15} FAMEs probably indicate that the non-pyrogenic OM is mainly microbial in origin (suggesting that C_{16} and C_{18} FAMEs are also of microbial origin in this case; cf. Miller et al., 2016).

The THM-GC-MS chromatogram of sample *GS3-h* was dominated by a series of FAMEs, with similar change length patterns as *Ilargi-h*, but with reduced intensity of the $>C_{20}$ FAMEs. Signal intensity is much lower, and presence of large peaks for alkenes suggests that the methylation was incomplete.

Synthesis and conclusions

The detectable OM in all samples is composed mainly of polymethylene chain aliphatic structures, recognized as MCC using Py-GC-MS and as FAMEs using THM-GC-MS. The origin of these compounds cannot be established easily. The alkadienes (Py-GC-MS), in combination with the presence of *iso*/*anteiso* C_{15} FAMEs (THM-GC-MS) with peaks that are larger than that of C_{14} FAME, suggest the presence of a considerable proportion of bacterial lipids. Even though part of this signal may correspond to old soil OM from the overlying soils, cave bacteria are more likely sources (Cox et al., 1989b; Cacchio et al., 2004; Blyth et al., 2008) and bat guano can produce MCC as well (Queffelec et al., 2018). Jex et al. (2014) showed a principal *in situ* (microbial) source of tetraether membrane lipids in diverse speleothems from glycerol dialkyl glycerol tetraetheral (GDGT) patterns. On the other hand, the detection of long-chain FAMEs with strong even-over-odd chain length predominance, ω-methoxy-FAMEs and some DAMEs might indicate some plant-derived aliphatic macromolecular and/or geopolymerized waxes. The presence of some plant-derived MCC is in accordance with Xie et al. (2003) and Blyth et al. (2007), which could use them to reconstruction vegetation communities. In the OM from the speleothems studied here, however, this aliphatic OM, which is the "matrix OM" in all analyzed samples, is probably of mixed sources (*ex situ* vegetation and *in situ* cave microorganisms and guano) with only a minor plant contribution.

The molecular fingerprint of the N-rich OM constituents indicates the presence of chitin/peptidoglycan in *Ilargi-h*, which is the sample with the highest molecular diversity. Here, apart from chitin (acetamide from Py-GC-MS), well-preserved protein is abundant (THM-GC-MS), and a source in soil OM is deemed very unlikely as other signals of relatively "fresh" soil OM, such as lignin and plant polysaccharide products, are negligible. They should probably be ascribed to the proteins in insectivorous guano (this is a hydroxylapatite layer), but contributions of animal protein (for instance bat collagen) and cave bacterial communities growing in guano (Wurster et al., 2015), cannot be excluded. For *Ilargi-h*, these results probably indicate dominance of lipids from the cave rather than from percolating water from the overlying soil. Whether this can be extrapolated for the much less diagnostic MCC and N-compound fingerprints of the other samples remains unknown. Note that speleothem excreta records such as that of bat guano are a valuable source of paleoenvironmental information when studied by means of stable isotope analysis ($\delta^{13}C$, $\delta^{15}N$; e.g., Wurster et al., 2010, Cleary & Onac, 2020), or even DNA sequencing by metabarconding that allows the identification of bat species (Walker et al., 2019), plant remains (Willerslev et al., 2003) and bacteria responsible of guano transformation (De Leon et al., 2018; Newman et al., 2018), opening possible lines of data cross-comparison to enhance the understanding of the mechanisms behind both stable isotope signals and variations in OM molecular composition.

The sample *GS3-h* is the sample with the second-highest contribution of polysaccharide derivatives (after *Ilargi-h*), and the second-lowest proportion of MCC. It seems that the samples from old erosion surfaces are enriched in guano remains, which is in line with the petrographic and SEM-EDS analyses of Martínez-Pillado et al. (2014) and also have OM that is relatively well-preserved, which is partly due to the local scale of OM production. The lack of acetamide in the pyrolyzate of sample *GS3-h* might indicate a source in non-insectivorous guano (*cf.* Blyth et al., 2015), but

the quality of the chromatogram in combination with the polar nature of acetamide may have deteriorated a possible chitin/peptidoglycan signal.

The samples with the strongest signals (Py-GC-MS, THM-GC-MS) of pyrogenic OM are *GS2-b*, *GS2-e*, and *GS2-r*. It may be coincidence that these samples originate from the same stalagmite, or that the position of *GS2* stimulated the accumulation of soot/smoke from anthropogenic fires in cave. The absence of fire evidence in the detritic sequence in the Galería del Silo and the Galería de las Estatuas, points to an accumulation of soot in the stalagmites mainly from the abundant fireplaces and *fumiers* present in the nearby El Portalón de Cueva Mayor archaeological site at the cave entrance (250 m away). Nevertheless, the use of torches instead of local hearths should be also considered as a possible source of soot. The chronology of the pyrogenic OM-rich black layers coincides with the most intense occupation periods of the El Portalón de Cueva Mayor archaeological site (Carretero et al., 2008; Pérez-Romero et al., 2017). Figure 1 shows the calculated ages of those samples with pyrogenic OM in the *Ilargi* stalagmite (*Ilargi-a* to *Ilargi-g*) (Martínez-Pillado et al., 2014), indicating that the first human activities within the karst using wood combustion began ca. 7,700 years ago, during the Neolithic period. The highest concentration of soot laminae occurs between 5,000 and 3,000 years ago, from the Chalcolithic to the Bronze Age period. All evidence is in agreement with the archaeo-sedimentary sequence of the El Portalón site (Carretero et al., 2008), where main archaeological units, Units *9* (Neolithic) to *3* (Bronze Age), overlap the chronologies of the black laminae.

In the case of *Ilargi-h* layer, the erosion surface related to this sample coincides with a hiatus of about 5.000 years, involving the boundary between the Pleistocene and the Holocene. The presence of chitin/peptidoglycan and proteins indicating a possible bat-guano layer can be correlated with Unit *9a* of El Portalón sequence, formed by a guano layer between 5 and 8 cm thick and dated at ca. 8,500 yr cal BP (Carretero et al., 2008). It also represents the transition from the Pleistocene (Unit 10) to the Holocene (Unit 9) and is characterized by the absence of human presence and activity at the site and the karst system (Carretero et al., 2008).

Interestingly, *Clon-b* has the largest proportion of cadalene and long-chain alkanes, possibly indicating terrestrial resins and plant lipids. The OM in this sample is strongly depleted in N-containing moieties and polysaccharides, suggesting that guano/microbial OM is a minor source. Alternatively, this lamina corresponds to material that was subjected to relatively strong diagenetic processes, and in fact the resin signature may partially correspond to kerogen in source rock. The other samples (*Ilargi-b*, *GS1-a*, and *GS3-d*) have pyrolyzate compositions with unexceptional proportions of aliphatic, pyrogenic and guano/microbial OM.

In conclusion, we have shown some interesting features of the OM in black laminae in speleothems from the Sierra de Atapuerca karst system that can lead to a better understanding of OM dynamics in cave environments. The OM types detected in black laminae include a long-chain aliphatic component (probably mixed microbial-/plant-derived), a nitrogen-rich component (from micro-organisms, guano and/or insect residues), and a pyrogenic component (probably anthropogenic). Exploring the complementarities with other methods seems to be a logical step in developing the precursor-product rationale of Py-GC-MS and THM-GC-MS and further assess their potential. The methods are useful screening tools to select samples for other (more time-consuming and/or more expensive) methods such as DNA sequencing. Once the sources can be established more reliably, these rapid and cost-efficient techniques may provide a useful tool for reconstructions based on speleothem composition.

ACKNOWLEDGMENTS

We are grateful to William Meredith, and an anonymous reviewer for their insightful comments.

Author statement: JK, AMC, and EI designed the study. JK and VMP performed the measurements and created the figures. VMP coordinated bridging environmental (JK, EI, AMC, and JSS) with archaeological proxies (AA, EI, and JLA). JK wrote the draft and all authors contributed to the final version.

REFERENCES

Aranburu, A., Martínez-Pillado, V., García, F., Arsuaga, J.L., Alcázar de Velasco, A., Bonmati, A., García, N., Gracia, F., Gómez, A., Lira, J., Lorenzo, C., Martínez, I., Ortega, A.I., Pablos, A., Pantoja, A., Quam, R., Sala, N., 2012. La variabilidad de los rellenos endokársticos de la Galería de Estatuas (Atapuerca, Burgos) y su caracterización paleoambiental. Avances de la Geomorfología en España, p. 397-400.

Arsuaga, J.L., Martínez, I., Gracia, A., Carretero, J.M., Lorenzo, C., García, N., Ortega, A.I., 1997. Sima de los Huesos (Sierra de Atapuerca). The site. Journal of Human Evolution, 33, 109-127. https://doi.org/10.1006/jhev.1997.0132

Arsuaga, J.L., Gómez-Olivencia, A., Sala, N., Martínez-Pillado, V., Pablos, A., Bonmatí, A., Pantoja-Pérez, A., Lira-Garrido, J., Alcázar de Velasco, A., Ortega, A.I., Cuenca-Bescós, G., García, N., Aranburu, A., Ruiz-Zapata, B., Gil-García, M.J., Rodríguez-Alvarez, X.P., Ollé, A., Mosquera, M., 2017. Evidence of paleoecological changes and Mousterian occupations at the Galería de las Estatuas site, Sierra de Atapuerca, norther Iberian plateau, Spain. Quaternary Research, 88, 345-367. https://doi.org/10.1017/qua.2017.46

Audra, P., De Waele, J., Bentaleb, I., Chroňáková, A., Krištůfek, V., D'Angeli, I.M., Carbone, C., Madonia, G., Vattano, M., Scopelliti, G., Cailhol, D., Vanara, N., Temovski, M., Bigot, J.-Y., Nobécourt, J.-C., Galli, E., Rull, F., Sanz-Arranz, A., 2019. Guano-related phosphate-rich minerals in European caves. International Journal of Speleology, 48(1), 75-105. https://doi.org/10.5038/1827-806X.48.1.2252

Bermúdez de Castro, J.M., Arsuaga, J.L., Carbonell, E., Rosas, A., Martínez, I., Mosquera, M., 1997. A hominid from Lower Pleistocene of Atapuerca, Spain: possible

ancestor to Neanderthals and modern humans. Science, 276, 1392-1395. https://doi.org/10.1126/science.276.5317.1392

Blyth, A.J., Frisia, S., 2008. Molecular evidence for bacterial mediation of calcite formation in cold high-altitude caves. Geomicrobiology Journal, 25, 101-111. https://doi.org/10.1080/01490450801934938

Blyth, A.J., Schouten, S., 2013. Calibrating the glycerol dialkyl glycerol tetraether temperature signal in speleothems, Geochimica et Cosmochimica Acta, 109, 312-328. https://doi.org/10.1016/j.gca.2013.02.009

Blyth, A.J., Watson J.S., 2009. Thermochemolysis of organic matter preserved in stalagmites: a preliminary study. Organic Geochemistry, 40, 1029-1031. https://doi.org/10.1016/j.orggeochem.2009.06.007

Blyth, A.J., Asrat, A., Baker, A., Gulliver, P., Leng, M.J., Genty, D., 2007. A new approach to detecting vegetation and land-use change using high-resolution lipid biomarker records in stalagmites. Quaternary Research, 68, 314-324. https://doi.org/10.1016/j.yqres.2007.08.002

Blyth, A.J., Baker, A., Collins, M.J., Penkman, K.E.H., Gilmour, M.A., Moss, J.S., Genty, D., Drysdale, R.N., 2008. Molecular organic matter in speleothems and its potential as an environmental proxy. Quaternary Science Reviews, 27, 905-921. https://doi.org/10.1016/j.quascirev.2008.02.002

Blyth, A.J., Watson, J.S., Woodhead, J., Hellstrom, J., 2010. Organic compounds preserved in a 2.9 million year old stalagmite from the Nullarbor Plain, Australia. Chemical Geology, 279, 101-105. https://doi.org/10.1016/j.chemgeo.2010.10.006

Blyth, A.J., Fuentes, D., George, S.C., Volk, H., 2015. Characterisation of organic inclusions in stalagmites using laser-ablation-micropyrolysis gas chromatography-mass spectrometry. Journal of Analytical and Applied Pyrolysis, 113, 454-463. https://doi.org/10.1016/j.jaap.2015.03.009

Boon, J.J., Pastorova, I., Botto, R.E., Arisz, P.W., 1994. Structural studies on cellulose pyrolysis and cellulose chars by PYMS, PYGCMS, FTIR, NMR and by wet chemical techniques. Biomass and Bioenergy, 7, 25-32. https://doi.org/10.1016/0961-9534(94)00044-T

Cacchio, P., Contento, R., Ercole, C., Cappuccio, G., Preite Martinez, M., Lepidi, A., 2004. Involvement of microorganisms in the formation of carbonate speleothems in Cervo Cave (L'Aquila—Italy). Geomicrobiology Journal, 21, 497-509. https://doi.org/10.1080/01490450490888109

Carbonell, E., Bermúdez de Castro, J.M., Arsuaga, J.L., Díez, J.C., Rosas, A., Cuenca Bescós, G., Sala, R., Mosquera, M., Rodríguez, X.P., 1995. Lower Pleistocene hominids and artefacts from Atapuerca — TD6 (Spain). Science, 269, 826-832. https://doi.org/10.1126/science.7638598

Carbonell, E., Bermúdez de Castro, J.M., Parés, J.M., Pérez-González, A., Cuenca-Bescós, G., Ollé, A., Mosquera, M., Huguet, R., Van der Made, J., Rosas, A., Sala, R., Vallverdú, J., García, N., Granger, D.E., Martinón-Torres, M., Rodríguez, X.P., Stock, G.M., Vergés, J. M., Allué, E., Burjachs, F., Cáceres, I., Canals, A., Benito, A., Díez, C., Lozano, M., Mateos, A., Navazo, M., Rodríguez, J., Rosell, J., Arsuaga, J.L., 2008. The first hominin of Europe. Nature, 452, 465-470. https://doi.org/10.1038/nature06815

Carretero, J.M., Ortega, A.I., Juez, L., Pérez-González, A., Arsuaga, J.L., Pérez-Martínez, R., Ortega, M.C., 2008. A Late Pleistocene-Early Holocene archaeological sequence of Portalón de Cueva Mayor (Sierra de Atapuerca, Burgos, Spain). Munibe (Antropologia-Arkeologia), 59, 67-80.

Challinor, J.M., 1991. The scope of pyrolysis methylation reactions. Journal of Analytical and Applied Pyrolysis, 20, 15-24. https://doi.org/10.1016/0165-2370(91)80059-H

Cleary, D.M., Onac, B.P., 2020. Using ratios in cave guano to assess past environmental changes. Geological Society, London, Special Publications, 507. https://doi.org/10.1144/SP507-2020-13

Costa, M., Rego, A., Ramos, V., Afonso, T.B., Freitas, S., Preto, M., Lopes, V., Vasconcelos, V., Magalhães, C., Leão, P.N., 2016. The conifer biomarkers dehydroabietic and abietic acids are widespread in Cyanobacteria. Scientific Reports, 6, 23436. https://doi.org/10.1038/srep23436

Cox, G., James, J.M., Osborne, R.A.L., Leggett, K.E.A., 1989a. Stromatolitic crayfish-like stalagmites. Proceedings of the University of Bristol Spelaeological Society, 18, 339-358.

Cox, G., James, J.M., Leggett, K.E.A., Osborne, R.A.L., 1989b. Cyanobacterially deposited speleothems: Subaerial stromatolites. Geomicrobiology Journal, 7, 245-252. https://doi.org/10.1080/01490458909377870

Dandurand, G., Duranthon, F., Jarr, M., Stratford, D.J., Bruxelles, L., 2019. Biogenic corrosion caused by bats in Drotsky's Cave (the Gcwihaba Hills, NW Botswana). Geomorphology, 327, 284-296. https://doi.org/10.1016/j.geomorph.2018.10.027

De Leeuw, J.W., Versteegh, G.J.M., van Bergen, P.F., 2006. Biomacromolecules of algae and plants and their fossil analogues. Plant Ecology, 182, 209-233. https://doi.org/10.1007/s11258-005-9027-x

De Leon, M.P., Montecillo, A.D., Pinili, D.S., Siringan, M.A.T., Park, D.-S., 2018. Bacterial diversity of bat guano from Cabalyorisa Cave, Mabini, Pangasinan, Philippines: A first report on the metagenome of Philippine bat guano. PLoS ONE, 13, e0200095. https://doi.org/10.1371/journal.pone.0200095

Fabbri, D., Helleur, R., 1999. Characterization of the tetramethylammonium hydroxide thermochemolysis products of carbohydrates, Journal of Analytical and Applied Pyrolysis, 49, 277-293. https://doi.org/10.1016/S0165-2370(98)00085-0

Fairchild, I.J., Baker, A., 2012. Speleothem science: From process to past environments. Wiley-Blackwell, Oxford, 450 p. https://doi.org/10.1002/9781444361094

Falguères, C., Bahain, J.J., Yokoyama, Y., Bischoff J.L., Arsuaga, J.L., Bermúdez De Castro, J.M., Carbonell, E., Dolo, J.M., 2001. Datation par RPE et U-Th des sites pléistocenes d´Atapuerca: Sima de los Huesos, Trinchera Dolina et Galería. Bilan géochronologique. L´Anthropologie, 105, 71-81. https://doi.org/10.1016/S0003-5521(01)80006-6

González-Pimentel, J.L., Miller, A.Z., Jurado, V., Laiz. L., Pereira, M.F.C., Saiz-Jimenez, C., 2018. Yellow colored mats form lava tubes of La Palma (Canary Islands. Spain) are dominated by metabolically active Actinobacteria. Scientific Reports, 8, 1944-1955. https://doi.org/10.1038/s41598-018-20393-2

González-Vila, F.J., Tinoco, P., Almendros, G., Martin, F., 2001. Pyrolysis–GC–MS analysis of the formation and degradation stages of charred residues from lignocellulosic biomass. Journal of Agricultural and Food Chemistry, 49, 1128-1131. https://doi.org/10.1021/jf0006325

Gupta, N.S., Cody, G.D., 2011. Characterization and identification of chitin from organisms. In: Gupta, N.S. (Ed.), Chitin: Formation and diagenesis, Springer, Dordrecht, p. 117-132. https://doi.org/10.1007/978-90-481-9684-5_6

Hatcher, P.G., Minard, R.D., 1995. Comment on the origin of benzenecarboxylic acids in pyrolysis methylation studies. Organic Geochemistry, 23, 991-994. https://doi.org/10.1016/0146-6380(95)00071-2

Hatcher, P.G., Clifford, D.J., 1997. The organic geochemistry of coal: from plant materials to coal. Organic Geochemistry, 27, 251-274. https://doi.org/10.1016/S0146-6380(97)00051-X

Heidke, I., Scholz, D., Hoffmann, T., 2018. Quantification of lignin oxidation products as vegetation biomarkers in speleothems and cave drip water. Biogeosciences, 15, 5831-5845. https://doi.org/10.5194/bg-15-5831-2018

Hou, J.C., Huang, Y.P., Tan, M.K., 2004. Carbon isotopic ratio of individual lignin moieties in stalagmite as a novel indicator of past C3/C4 plant variations. American Geophysical Union, Fall Meeting, Abstract ID PP43A-0607.

Huang, X.Y., Cui, J.W., Pu, Y., Huang, J., Blyth, A.J., 2008. Identifying "free" and "bound" lipid fractions in stalagmite samples: An example from Heshang Cave, Southern China. Applied Geochemistry, 23, 2589-2595. https://doi.org/10.1016/j.apgeochem.2008.05.008

Jex, C.N., Blyth, A.J., Baker, A., McDonald, J.A., Woltering, M., Khan, S.J., 2014. Characterising the transport and preservation of microbial tetraether membrane lipids in karst systems. American Geophysical Union, Fall Meeting, San Francisco, Abstract ID PP43B-2096. https://doi.org/10.13140/2.1.2414.8800

Kaal, J., Filley, T., 2016. Novel molecular proxies for inferring pyrogenic black carbon oxidation state using thermally assisted hydrolysis and methylation (THM-GC-MS) with ^{13}C-labeled tetramethylammonium hydroxide (TMAH). Journal of Analytical and Applied Pyrolysis, 121, 146-154. https://doi.org/10.1016/j.jaap.2016.07.015

Kaal, J., Brodowski, S., Baldock, J.A., Nierop, K.G.J., Cortizas, A.M., 2008. Characterisation of aged black carbon using pyrolysis-GC/MS, thermally assisted hydrolysis and methylation (THM), direct and cross-polarisation ^{13}C nuclear magnetic resonance (DP/CP NMR) and the benzenepolycarboxylic acid (BPCA) method. Organic Geochemistry, 39, 1415-1426. https://doi.org/10.1016/j.orggeochem.2008.06.011

Kaal, J., Nierop, K.G.J., Martínez Cortizas, A., 2009. Characterisation of aged charcoal using a coil probe pyrolysis-GC/MS method optimised for Black Carbon. Journal of Analytical and Applied Pyrolysis, 85, 408-416. https://doi.org/10.1016/j.jaap.2008.11.007

Kaal, J., Wagner, S., Jaffé, R., 2016. Molecular properties of ultrafiltered dissolved organic matter and dissolved black carbon in headwater streams as determined by pyrolysis-GC–MS. Journal of Analytical and Applied Pyrolysis, 118, 181-191. https://doi.org/10.1016/j.jaap.2016.02.003

Kaal, J. Martínez-Cortizas, A., Biester, H., 2017. Downstream changes in molecular composition of DOM along a headwater stream in the Harz Mountains (Central Germany) as determined by FTIR, Pyrolysis-GC–MS and THM-GC–MS. Journal of Analytical and Applied Pyrolysis, 126, 50-61. https://doi.org/10.1016/j.jaap.2017.06.025

Kaal, J., Plaza, C., Pérez-Rodríguez, M., Biester, H., 2020. Towards understanding ecological disaster in the Harz Mountains (Central Germany) by carbon tracing: pyrolysis-GC-MS of biological tissues and their water-extractable organic matter (WEOM). Analytical Pyrolysis Letters 8, 1-17. https://pyrolyscience.com/apl008/

Kaneda, T., 1991. Iso- and anteiso-fatty acids in bacteria: biosynthesis, function, and taxonomic significance. Microbiological Reviews, 55, 288-302. https://doi.org/10.1128/MR.55.2.288-302.1991

Keeling, C.I., Bohlmann, J., 2006. Diterpene resin acids in conifers. Phytochemistry, 67, 2415-2423. https://doi.org/10.1016/j.phytochem.2006.08.019

Knicker, H., del Río, J.C., Hatcher, P.G., Minard, R.D., 2001. Identification of protein remnants in insoluble geopolymers using TMAH thermochemolysis/GC-MS. Organic Geochemistry, 32, 397-409. https://doi.org/10.1016/S0146-6380(00)00186-8

Kolattukudy, P.E., 2001). Polyesters in higher plants. Advances in Biochemical Engineering/Biotechnology, 71, 1-49. https://doi.org/10.1007/3-540-40021-4_1

Lavoie, K., Witer, A.S., Read, K.J.H., Hughes, E.M., Spilde, M.N., Northup, D.E., 2017. Comparison of bacterial communities from lava cave microbial mats to overlying surface soils from Lava Beds National Monument, USA. PLoS One, 12, e0169339. https://doi.org/10.1371/journal.pone.0169339

Lejay, M., Alexis, M.A., Quénéa, K., Anquetil, C., Bon, F., 2019. The organic signature of an experimental meat-cooking fireplace: The identification of nitrogen compounds and their archaeological potential. Organic Geochemistry, 138, 103923. https://doi.org/10.1016/j.orggeochem.2019.103923

Martínez Pillado, V., Aramburu Artano, A., Arsuaga, J.L., Ruiz Zapata, M.B., Gil García, M.J., Stoll, H., Yusta Arnal, I., Iriarte, E., Carretero, J.M., Edwards, R.L., Cheng, H., 2014. Upper Pleistocene and Holocene paleoenvironmental records in Cueva Mayor karst (Atapuerca, Spain) from different proxies: speleothem crystal fabrics, palynology, and archaeology. International Journal of Speleology, 43(1), 1-14. https://doi.org/10.5038/1827-806X.43.1.1

Miller, A.Z., de la Roca, J.M., Jiménez-Morillo, N.T., Pereira, M.F.C., González-Pérez, J.A., Calaforra, J.M., Saiz-Jiménez, C., 2016. Analytical pyrolysis and stable isotope analyses reveal past environmental changes in coralloid speleothems from Easter Island (Chile). Journal of Chromatography A, 1461, 144-152. https://doi.org/10.1016/j.chroma.2016.07.038

Miller, A.Z., de la Rosa, J.M., Jiménez-Morillo, N.T., Pereira, M.F.C., González-Pérez, J.A., Knicker, H., Sáiz-Jiménez, C., 2020. Impact of wildfires on subsurface volcanic environments: New insights into speleothem chemistry. Science of the Total Environment, 698, 134321. https://doi.org/10.1016/j.scitotenv.2019.134321

Miltner, A., Zech, W., 1997. Effects of minerals on the transformation of organic matter during simulated fire-induced pyrolysis. Organic Geochemistry, 26, 175-182. https://doi.org/10.1016/S0146-6380(97)00002-8

Newman, M.M., Kloepper, L.N., Duncan, M., McInroy, J.A., Kloepper, J.W., 2018. Variation in Bat guano bacterial community composition with depth. Frontiers in Microbiology, 9, 914. https://doi.org/10.3389/fmicb.2018.00914

Nierop, K.G.J., Filley, T.R., 2007. Assessment of lignin and (poly-)phenol transformations in oak (*Quercus robur*) dominated soils by ^{13}C-TMAH thermochemolysis. Organic Geochemistry, 38, 551-565. https://doi.org/10.1016/j.orggeochem.2006.12.007

Nierop, K.G.J., Verstraten, J.M., 2004. Rapid molecular assessment of the bioturbation extent in sandy soil horizons under pine using ester-bound lipids by on-line thermally assisted hydrolysis and methylation-gas chromatography/mass spectrometry. Rapid Communications in Mass Spectrometry, 18, 1081-1088. https://doi.org/10.1002/rcm.1449

Nip, M., Tegelaar, E.W., Brinkbuis, H., de Leeuw, J.W., Schenck, P.A., Holloway, P.J., 1986. Analysis of modern and fossil plant cuticles by Curie point Py-GC and Curie point Py-GC-MS: Recognition of a new, highly aliphatic and resistant biopolymer. Organic Geochemistry, 10, 769-778. https://doi.org/10.1016/S0146-6380(86)80014-6

Ortega Martínez, A.I., 2009. La evolución geomorfológica del karst de la Sierra de Atapuerca (Burgos) y su relación con los yacimientos pleistocenos. Unpublished PhD Dissertation, Universidad de Burgos, 624 p.

Pastorova, I., Botto, R.E., Arisz, P.W., Boon, J.J., 1994. Cellulose char structure: a combined analytical Py-GC-MS, FTIR, and NMR study. Carbohydrate Research, 262, 27-47. https://doi.org/10.1016/0008-6215(94)84003-2

Pérez-Romero, A., Iriarte, E., Galindo-Pellicena, M.A., García-González, R., Rodríguez, L., Castilla, M., Francés-Negro, M., Santos, E., Valdiosera, C., Arsuaga, J.L., Alday, A., Carretero, J.M., 2017. An unusual pre-bell beaker copper age cave burial context from El Portalón de Cueva Mayor site (Sierra de Atapuerca, Burgos). Quaternary International, 433, 142-155. https://doi.org/10.1016/j.quaint.2015.06.063

Queffelec, A., Bertran, P.I., Bos, T., Lemée, L., 2018. Mineralogical and organic study of bat and chough guano: implications for guano identification in ancient context. Journal of Cave and Karst Studies, 80, 1-17. https://doi.org/10.4311/2017ES0102

Quénéa, K., Derenne, S., González-Vila, F.J., González-Pérez, J.A., Mariotti, A., Largeau, C., 2006. Double-shot pyrolysis of the non-hydrolysable organic fraction isolated from a sandy forest soil (Landes de Gascogne, South-West France): Comparison with classical Curie point pyrolysis. Journal of Analytical and Applied Pyrolysis, 76, 271-279. https://doi.org/10.1016/j.jaap.2005.12.007

Ratledge, C., 1997. Microbial lipids. In: Rehm, H.-J., Reed, G. (Eds.), Biotechnology: Products of secondary metabolism (2nd ed.), Vol. 7, VCH Verlagsgesellschaft mbH, p. 133-197. https://doi.org/10.1002/9783527620890.ch4

Ratledge, C., Wilkinson, S.G., 1998. Microbial lipids. Academic Press, London, 963 p.

Riquelme, C., Rigal, F., Hathaway, J.J.M., Northup, D.E., Spilde, M.N., Borges, P.A.V., Gabriel, R., Amorim, I.R., Dapkevicius, M.L.N.E., 2015. Cave microbial community composition in oceanic islands: Disentangling the effect of different colored mats in diversity patterns of Azorean lava caves. FEMS Microbiology Ecology, 91, 1-12. https://doi.org/10.1093/femsec/fiv141

Romero-Sarmiento, M.-F., Riboulleau, A., Vecoli, M., Versteegh, G.J.M., 2010. Occurrence of retene in upper Silurian–lower Devonian sediments from North Africa: Origin and implications. Organic Geochemistry, 41, 302-306. https://doi.org/10.1016/j.orggeochem.2009.10.003

Rousseau, L., Laafar, S., Pepe, C & DeLumley, H., 1995. Sterols as biogeochemical markers — results from ensemble-B of the stalagmitic floor, Grotte-du-Lazaret, Nice, France. Quaternary Science Reviews, 14, 51-59. https://doi.org/10.1016/0277-3791(94)00111-N

Rushdi, A.I., Clark, P.U., Mix, A.C., Ersek, V., Simoneit, B.R.T., Cheng, H., Edwards, R.L., 2011. Composition and sources of lipid compounds in speleothem calcite from southwestern Oregon and their paleoenvironmental implications. Environmental Earth Sciences, 62, 1245-1261. https://doi.org/10.1007/s12665-010-0613-4

Sáiz-Jiménez, C., 1994. Analytical pyrolysis of humic substances: pitfalls, limitations, and possible solutions. Environmental Science and Technology, 28, 1773-1780. https://doi.org/10.1021/es00060a005

Sáiz-Jiménez, C., de Leeuw, J.W., 1986. Lignin pyrolysis products: Their structures and their significance as biomarkers. Organic Geochemistry, 10, 869-876. https://doi.org/10.1016/S0146-6380(86)80024-9

Sanjurjo-Sánchez, J., Arce-Chamorro, C., Vidal Romaní,, J.R., Vaqueiro-Rodríguez, M., Barrientos, V., Kaal, J., 2021. On the genesis of aluminium-rich speleothems in a granite cave of NW Iberia. International Journal of Speleology, 50(1), 25-40. https://doi.org/10.5038/1827-806X.50.1.2358

Scholz, D., Hoffmann, D.L., 2011. StalAge - An algorithm designed for construction of speleothem age models. Quaternary Geochronology, 6, 369-382. https://doi.org/10.1016/j.quageo.2011.02.002

Spaccini, R., Song, X.Y., Cozzolino, V., Piccolo, A., 2013. Molecular evaluation of soil organic matter characteristics in three agricultural soils by improved off-line thermochemolysis: The effect of hydrofluoric acid demineralisation treatment. Analytica Chimica Acta, 802, 46-55. https://doi.org/10.1016/j.aca.2013.09.031

Stankiewicz, B.A., van Bergen, P.F., Duncan, I.J., Carter, J.F., Briggs, D.E.G., Evershed, R.P., 1996. Recognition of chitin and proteins in invertebrate cuticles using analytical pyrolysis/gas chromatography and pyrolysis/gas chromatography/mass spectrometry. Rapid Communications in Mass Spectrometry, 10, 1747-1757. https://doi.org/10.1002/(SICI)1097-0231(199611)10:14%3C1747::AID-RCM713%3E3.0.CO;2-H

Tegelaar, E.W., De Leeuw, J.W., and Holloway, P.J., 1989. Some mechanisms of flash pyrolysis of naturally occurring higher plant polyesters. Journal of Analytical and Applied Pyrolysis, 15, 289-295. https://doi.org/10.1016/0165-2370(89)85041-7

Van Aarssen, B.G.K., de Leeuw, J.W., Collinson, M., Boon, J.J., Goth, K., 1994. Occurrence of polycadinene in fossil and recent resins. Geochimica et Cosmochimica Acta, 58, 223-229. https://doi.org/10.1016/0016-7037(94)90459-6

Vergès, J.M., Fontanals, M., Morales, J.I., Allué, E., Carrancho, A., Euba, I., Expósito, I., Lozano, M., Marsal, R., Martín, P., Oms, X., Rodríguez, A., 2016. El Mirador Cave (Sierra de Atapuerca, Burgos, Spain): a whole perspective. Quaternary International, 414, 236-243. https://doi.org/10.1016/j.quaint.2016.01.044

Walker, F.M., Tobin, A., Simmons, N.B., Sobek, C.J., Sanchez, D.E., Chambers, C.L., Fofanov, V.Y., 2019. A fecal sequel: Testing the limits of a genetic assay for bat species identification. PLoS ONE, 14, e0224969. https://doi.org/10.1371/journal.pone.0224969

Willerslev, E., Hansen, A.J., Binladen, J., Brand, T.B., Gilbert, M.T.P., Shapiro, B., Bunce, M., Wiuf, C., Gilichinsky, D.A., Cooper, A., 2003. Diverse plant and animal genetic records from Holocene and Pleistocene sediments. Science, 300, 791-795. https://doi.org/10.1126/science.1084114

Willey, J.M., Sherwood, L., Prescott, L.M., Woolverton, C.J., 2008. Microbiology. McGraw-Hill, New York, 1088 p.

Wimsatt, W.A., 1970. The biology of bats. Academic Press, New York.

Wurster, C.M., McFarlane, D.A., Bird, M.I., Ascough, P., Athfield, N.B., 2010. Stable isotopes of subfossil bat guano as a long-term environmental archive: insights from a Grand Canyon cave deposit. Journal of Cave and Karst Studies, 72, 111-121. https://doi.org/10.4311/jcks2009es0109

Wurster, C.M., Munksgaard, N., Zwart, C., Bird, M., 2015. The biogeochemistry of insectivorous cave guano: a case study from insular Southeast Asia. Biogeochemistry, 124, 163-175. https://doi.org/10.1007/s10533-015-0089-0

Wynn, P.M., Brocks, J.J., 2014. A framework for the extraction and interpretation of organic molecules in speleothem carbonate. Rapid Communications in Mass Spectrometry, 28, 845-854. https://doi.org/10.1002/rcm.6843

Xie, S., Yi, Y., Huang, J., Hu, C., Cai, Y., Collins, M., Baker, A., 2003. Lipid distribution in a subtropical southern China stalagmite as a record of soil ecosystem response to paleoclimate change. Quaternary Research, 60, 340-347. https://doi.org/10.1016/j.yqres.2003.07.010

Yang, H., Ding, W., Zhang, C.L., Ding, W., Zhang, C.L., Wu, X., Ma, X., He, G., Huang, J., Xie, S., 2011. Occurrence of tetraether lipids in stalagmites: implications for sources and GDGT-based proxies. Organic Geochemistry, 42, 108-115. https://doi.org/10.1016/j.orggeochem.2010.11.006